Available online at www.sciencedirect.com
ScienceDirect
Acta Materialia 55 (2007) 1299–1308
Acta MATERIALIA
www.actamat-journals.com

Strengthening mechanisms in aluminum containing coherent Al_3Sc precipitates and incoherent Al_2O_3 dispersoids

Richard A. Karnesky [a], Liang Meng [b], David C. Dunand [a,*]

[a] Department of Materials Science and Engineering, 2220 North Campus Drive, Northwestern University, Evanston, IL 60208-3108, USA
[b] Department of Materials Science and Chemical Engineering, Zhejiang University, Hangzhou 310027, PR China

Received 25 July 2006; accepted 12 October 2006
Available online 15 December 2006

Abstract

Dispersion-strengthened-cast aluminum (DSC-Al), consisting of a coarse-grained aluminum matrix containing two populations of particles (30 vol.% of 300 nm Al_2O_3 incoherent dispersoids and 0.2–0.3 vol.% of 6–60 nm coherent Al_3Sc precipitates), was studied. At ambient and elevated temperatures, both populations of particles contribute to strengthening. At 300 °C, creep threshold stresses are considerably higher than for control materials with a single population of either Al_2O_3 dispersoids or Al_3Sc precipitates. This synergistic effect is modeled by considering dislocations pinned at the departure side of incoherent Al_2O_3 dispersoids (detachment model) and simultaneously subjected to elastic interactions from neighboring coherent Al_3Sc precipitates.

Keywords: Metal matrix composites; Precipitation; Aluminum alloys; Creep; Zirconium

1. Introduction

Incoherent ceramic dispersoids (with size below ~1 μm) distributed within a coarse-grained metallic matrix provide high strength at ambient and elevated temperatures, as they impede dislocation glide and climb [1]. Choosing chemically stable and coarsening-resistant submicron dispersoids such as Al_2O_3 allows for dispersion-strengthened aluminum with creep-resistance to high temperatures (500 °C and above [2–10]). When creep is controlled by dislocation motion, the minimum strain rate, $\dot{\varepsilon}$, of dispersion-strengthened aluminum can be described by a power-law equation [11]:

$$\dot{\varepsilon} = A_{ap}\sigma^{n_{ap}} \exp\left(-\frac{Q_{ap}}{RT}\right), \quad (1)$$

where subscript ap stands for "apparent", A is a dimensionless constant (calculated from the diffusion coefficient, shear modulus, test temperature, Burgers vector and grain size of the matrix), σ is the applied stress, n is the matrix stress exponent (which is mechanism- and material-dependent), Q is the matrix creep activation energy, R is the ideal gas constant and T is the absolute temperature. Dispersion-strengthened aluminum exhibits much lower strain rates than pure aluminum in the low-stress regime, as well as higher apparent stress- and temperature-dependence (n_{ap} and Q_{ap}). This behavior can be modeled by introducing in Eq. (1) a threshold stress, σ_{th}, below which creep is not measurable experimentally:

$$\dot{\varepsilon} = A(\sigma - \sigma_{th})^n \exp\left(-\frac{Q}{RT}\right). \quad (2)$$

For dispersion-strengthened alloys, the origin of the threshold stress has been shown to be the detachment of the dislocations from the incoherent dispersoids [12]. This detachment model, some versions of which consider thermally activated detachment of dislocations [13], was recently modified to take into account the effect of dislocation pile-up in dispersion-strengthened-cast aluminum (DSC-

* Corresponding author. Tel.: +1 847 491 5370; fax: +1 847 467 2269.
E-mail address: dunand@northwestern.edu (D.C. Dunand).

1359-6454/$30.00
doi:10.1016/j.actamat.2006.10.004

Al) consisting of unalloyed aluminum with high volume fractions (>20%) of submicron alumina dispersoids [14].

Whereas dispersoids are typically added *ex situ* in aluminum by powder or liquid metallurgy and are thus incoherent with the matrix, precipitates are created *in situ* in aluminum by heat-treatment and can remain coherent when their size is small. The low precipitate volume fractions achievable in conventionally cast aluminum alloys dictate that the precipitates must remain nanometric in size to maintain their effectiveness against dislocation motion. For long-term creep resistance, alloying additions producing slow-coarsening precipitates are thus essential and among various candidates [15], scandium has been the focus of recent research for creep-resistant aluminum alloys [16–24].

Homogenized, dilute Al–Sc alloys (with Sc concentration below the maximum solubility of 0.23 at.%) can be aged to form a high number density of coherent $L1_2$ Al_3Sc precipitates which show negligible coarsening rates up to about 300 °C [25–31]. Zirconium can partially substitute for Sc in precipitates, forming coherent $L1_2$ $Al_3(Sc_{1-x}Zr_x)$ precipitates with improved coarsening resistance up to at least 350 °C. This is due to the much lower diffusivity of Zr as compared to Sc, and to Zr partitioning to the precipitate interface which inhibits Sc diffusion [32–38]. Coherent precipitates have been shown to increase the creep-resistance of cast, coarse-grained Sc-containing alloys with additions of Mg, Zr, Ti, or rare-earth elements by introducing a threshold stress [16–24]. Because these precipitates are coherent, detachment cannot be invoked as a threshold mechanism. Previous studies showed that precipitate cutting is not operative, leaving precipitate bypass by dislocation climb as the most likely threshold mechanism [17–20,39]. A small threshold stress (~2% of the Orowan stress) is expected for this general-climb mechanism, independently of precipitate radius [19,20,39,40]. However, these dilute Al–Sc alloys show a threshold stress increasing with precipitate radius to much higher fractions of the Orowan stress (up to 70%) [19]. This behavior was explained by extending the general-climb model to include back-stresses acting on the dislocations, originating from the lattice and modulus mismatches between the aluminum matrix and the coherent Al_3Sc precipitates [39].

The present research examines DSC-Al–Sc(–Zr) alloys which contain two distinct populations of dislocation-impeding particles: a high volume fraction of submicron, incoherent Al_2O_3 dispersoids and a low volume fraction of nanometer-size, coherent Al_3Sc or $Al_3(Sc_{1-x}Zr_x)$ precipitates. The microhardness and compressive properties at ambient temperature and the creep-resistance at elevated temperatures are measured for these alloys and compared to existing data on control alloys containing only one population of particles, i.e., Al–Sc(–Zr) alloys (with Al_3Sc or $Al_3(Sc_{1-x}Zr_x)$ precipitates but without Al_2O_3 dispersoids) and DSC-Al (with Al_2O_3 dispersoids but without Al_3Sc or $Al_3(Sc_{1-x}Zr_x)$ precipitates). Existing models for the strengthening effect of each type of particles are combined to explain the synergetic strengthening found in the DSC-Al–Sc(–Zr) alloys with both types of particles.

2. Experimental methods

2.1. Materials preparation

An Al–0.11 at.% Sc (Al–0.18 wt.%Sc) alloy was created by dilution of small quantities of Al–0.5 wt.%Sc master alloy to 99.9% pure Al. The melt was cast in an alumina crucible and solidified in air. This alloy is referred to as Al–Sc in the following. An Al–0.08 at.%Sc–0.03 at.%Zr alloy (Al–0.13 wt.% Sc–0.10 wt.%Zr, referred to as Al–Sc–Zr) was cast from 99.99% Al, an Al–1.7 wt.%Sc master alloy and an Al–4.4 wt.%Zr master alloy. This material was melted in a zirconia-coated alumina crucible, stirred and poured into a boron-nitride-coated graphite mold resting on a copper plate. The typical grain size of the resulting alloys was 1–2 mm. Alloy compositions were determined by plasma emission spectroscopy by Luvak Inc. (Boylston, MA, USA).

Chesapeake Composites Corp. (New Castle, DE, USA) supplied several dispersion-strengthened-cast (DSC) billets produced by melt infiltration of preforms of Al_2O_3 particles with a 0.3 μm average size [41]. Two billets, referred to as DSC-Al–Sc and DSC-Al–Sc–Zr, were fabricated from the above Al–Sc and Al–Sc–Zr cast alloys. Three control billets, all referred to as DSC-Al, were fabricated from 99.98% pure Al. All DSC billets contained 30.1 ± 0.2 vol.% Al_2O_3 dispersoids, as determined from mass density measurements by the Archimedes method.

The unalloyed DSC-Al specimens were tested in the as-cast condition. Aging treatments for the other alloys consisted of homogenization at 640 °C in air for 24 h for the alloys without Zr and for 120 h for the alloys with Zr (due to the lower diffusivity), water-quenching to ambient temperature, aging in air at 300–450 °C for various times, terminated by a water-quench to ambient temperature.

2.2. Conductivity measurements

Electrical conductivity was measured at ambient temperature on coupons (with at least 11 mm diameter, 5 mm width and polished to a 1 μm surface finish) aged in air at 300 °C for various times after homogenization, using an eddy-current instrument (Sigmatest 2.069, from Foerster Instruments Inc. (Pittsburgh, PA)). Both sides of the coupons were measured at operating frequencies of 60, 120, 240, 480, and 960 kHz. Errors reported are for one standard deviation from the mean value.

2.3. Mechanical properties

Vickers microhardness measurements were performed with a 500 g load for 5 s on coupons (with size at least $5 \times 5 \times 3$ mm^3 and polished to a 1 μm surface finish) aged in air at 300 and 350 °C for various times after homogeni-

zation. Errors reported are for one standard deviation from the mean value.

Cylindrical DSC specimens (with 8.10 mm diameter and 16.10 mm length) were electro-discharge machined with their axes parallel to that of the cast billet. DSC-Al–Sc specimens, homogenized and aged at 350 °C for 24 h and 450 °C for 60 h, were tested in uniaxial compression at ambient temperature, using a constant rate of crosshead displacement of 1.0 mm/min. Compressive creep experiments at constant load were performed in air at 300 and 350 °C for the three DSC alloys, using a three-zone, resistively heated furnace with a temperature stability of ±1 °C. A superalloy compression-cage was used with boron-nitride-lubricated alumina platens. The platen displacement, transmitted by an extensometer connected to a linear voltage displacement transducer, was continuously monitored and recorded by computer to 2.5 μm resolution. At any given stress level, sufficient time was allowed to establish a minimum creep rate, as determined by weighted linear regression. If the sample had not failed, the load was increased. Therefore, a single specimen could be utilized to obtain minimum creep rates at multiple stress levels. Typically, steady-state creep rate was determined after ~2% strain, over approximately the last 0.5% strain range. Different aging treatments were utilized for the DSC-Al–Sc-(–Zr) specimens, in order to study the effects of distribution and size of $Al_3(Sc_{1-x}Zr_x)$ precipitates. Some specimens were used repeatedly in creep tests after intermediate aging treatments, as described later.

3. Results

3.1. Microhardness and strength at ambient temperature

Fig. 1 shows the evolution of microhardness with aging time at 300 and 350 °C for all alloys in this study. The four expected regimes for precipitation strengthening (due to formation of Al_3Sc or $Al_3(Sc_{1-x}Zr_x)$ precipitates) can be observed sequentially: (i) a short region where hardness remains equal to the as-cast value (incubation); (ii) a rapid increase in hardness (under-aging); (iii) a plateau in hardness values (peak-aging); and (iv) a slow decrease in hardness (over-aging).

In Al–Sc, peak-aging occurs after ~2 h at 300 °C and ~0.25 h at 350 °C. Also, onset of over-aging occurs earlier at 350 °C. The over-aged microhardness appears stable for times longer than 16 h at 300 °C or 6 h at 350 °C. The peak hardness for aging at 350 °C is lower than that at 300 °C by about 16%, while the over-aged hardness at 350 °C is lower than that at 300 °C by about 31%.

Al–Sc–Zr achieves peak-aging after ~4 h at 300 °C and ~0.3 h at 350 °C, the same times as Al–Sc within experimental error. The peak hardness is slightly lower in Al–Sc–Zr at both aging temperatures. Over-aging in Al–Sc–Zr does not cause as much of a decrease of hardness as in Al–Sc and the hardness remains stable when aged for 1536 h (64 days).

In DSC-Al–Sc, hardness peaks after ~4 h at 300 °C and ~0.4 h at 350 °C. The hardness decreases slightly after achieving its peak value and then remains almost constant for over 384 h (16 days) at either 300 or 350 °C. The time span of this plateau is longer than a creep experiment, so precipitate radii can safely be assumed to remain constant through a creep test. The peak hardness for aging at 350 °C is the same as at 300 °C, within experimental error, while the stable hardness for aging at 350 °C is lower than that at 300 °C by about 14%. The DSC-Al–Sc peak hardness is about three times higher than that of Al–Sc when aged at 350 °C and about twice as high when aged at 300 °C. This illustrates the hardening contribution from the Al_2O_3 dispersoids, which is independent of aging time or temperature.

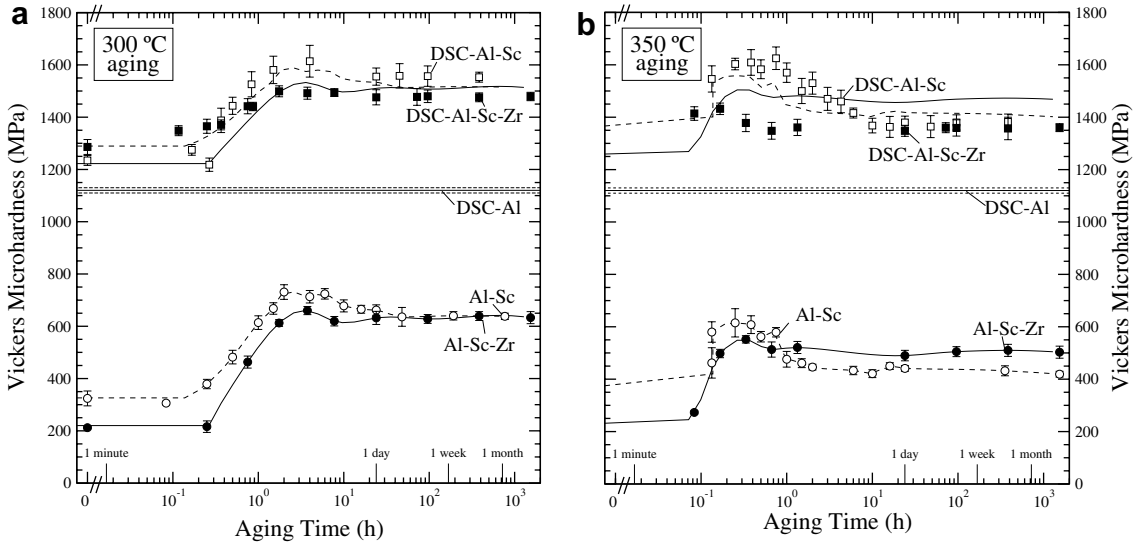

Fig. 1. Vickers microhardness as a function of aging time at (a) 300 °C and (b) 350 °C. The curves for the DSC-Al–Sc and DSC-Al–Sc–Zr were calculated from Eq. (3) with $k = 1.3$, using best-fit curves for DSC-Al, Al–Sc and Al–Sc–Zr.

DSC-Al–Sc–Zr reaches peak-aging after ~2 h at 300 °C and after 0.2 h at 350 °C. Both of these times, though shorter, are within experimental error of the peak-aging times for DSC-Al–Sc. The peak hardness of DSC-Al–Sc–Zr is lower than that of DSC-Al–Sc by ~7% when aged at 300 °C and ~12% when aged at 350 °C. At 300 °C, hardness remains constant at the peak value when over-aged for as long as 1536 h (64 days), as with Al–Sc–Zr. Thus, the assumption that precipitate size is constant through a creep experiment is safe. Although there is little change in hardness when aged at 350 °C, DSC-Al–Sc–Zr is always harder than the as-homogenized alloy. This trend of lower hardness for higher aging temperatures was previously observed for Al–Sc–Zr alloys and was attributed to coarsening [20].

In Fig. 2(a) and (b), the normalized electrical conductivity, $\sigma_n(t) = (\sigma(t) - \sigma(t=0))/(\sigma(t=t_{max}) - \sigma(t=0))$, is plotted against aging time at 300 °C, where $\sigma(t)$ is the electrical conductivity at time $t = 0$ (no aging), t or t_{max} (longest aging time). The conductivity increases with aging, as the concentration of Sc and Zr atoms in solid-solution within the matrix decreases from the as-homogenized values due to precipitation. The curves of the DSC alloys overlap those of their matrix alloys, indicating that the Al_2O_3 dispersoids do not significantly modify the nucleation and growth of Al_3Sc or $Al_3(Sc_{1-x}Zr_x)$ precipitates.

The compressive yield stress, as measured by the first detectable deviation from the linear portion of the stress–strain curve, is 350 ± 10 MPa for DSC-Al aged at 350 °C for 24 h and 270 ± 10 MPa when aged at 450 °C for 60 h. The 0.2% proof stresses were 357 ± 2 and 275 ± 2 MPa, respectively. The ultimate compressive strengths were 609 and 500 MPa. These strengths are slightly higher than those reported for DSC-Al with 32 vol.% Al_2O_3 [42]. Direct comparison is not possible, since this previous alloy had been extruded and thus exhibited a very small grain size (0.88 μm) contributing to its strength. However, the drop in strength observed upon over-aging in the present alloys is a clear indication that precipitates contribute to ambient-temperature strength. The Young's modulus, found from the elastic slope of the stress–strain curve, is 103 ± 5 GPa for both samples, in good agreement with previous results on DSC-Al without alloying additions to the matrix [41,42].

3.2. Creep properties

Fig. 3(a) displays the steady-state creep behavior at 300 °C – plotted as minimum creep rate, $\dot{\varepsilon}$, vs. applied stress, σ, on double-logarithmic axes – for DSC-Al, DSC-Al–Sc (aged at 300 °C for 24 h) and DSC-Al–Sc–Zr (aged at 350 °C for 17 h). The aging treatments were selected to yield approximately the same 3 nm precipitate radius for both Sc-containing alloys, based on measurements reported in Refs. [43,44]. All three alloys have high apparent stress exponents, indicative of a threshold stress. DSC-Al–Sc is significantly more creep-resistant than Sc-free DSC-Al. DSC-Al–Sc–Zr is less creep-resistant than DSC-Al–Sc, but still more creep-resistant than DSC-Al at strain rates below about 10^{-6} s^{-1}.

After creep testing, the above DSC-Al–Sc sample, which had been aged at 300 °C for 24 h prior to testing, was reaged at 450 °C for 24 h and creep tested again. Finally, the same sample was subjected to a third aging treatment at 450 °C for 24 h and creep tested for a third time. Creep results are plotted in Fig. 3(b), which shows that creep-resistance decreases with increased aging, as expected if precipitates are coarsening during the second and third heat-treatments. Nevertheless, the over-aged DSC-Al–Sc sample which had been subjected to three aging treatments remained more creep-resistant than the precipitate-free DSC-Al samples.

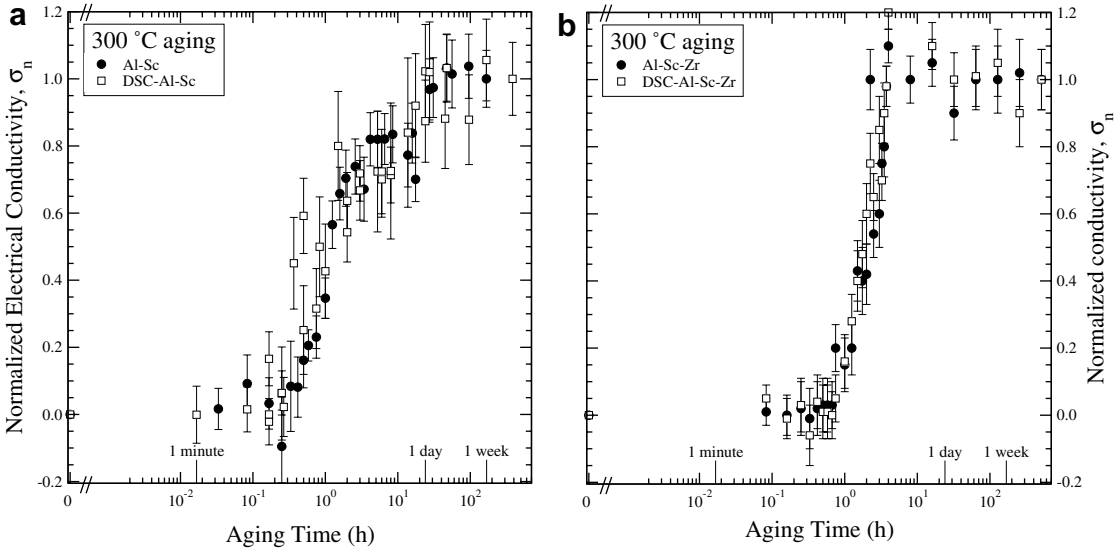

Fig. 2. Normalized electrical conductivity as a function of aging time at 300 °C for (a) DSC-Al–Sc and Al–Sc and (b) DSC-Al–Sc–Zr and Al–Sc–Zr.

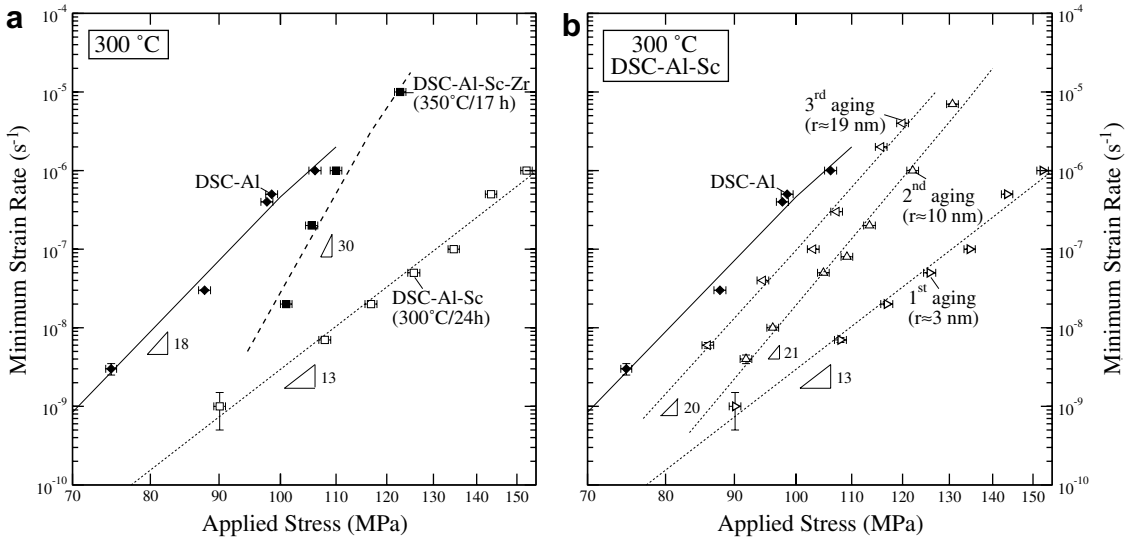

Fig. 3. Stress dependence of minimum compressive creep strain rate at 300 °C. (a) For DSC-Al, DSC-Al–Sc and DSC-Al–Sc–Zr, the latter two alloys being aged to achieve Al_3Sc and $Al_3(Sc_{1-x}Zr_x)$ precipitates with the same radius of ~3 nm. (b) For a DSC-Al–Sc sample subjected to three successive aging treatments to coarsen Al_3Sc precipitates (estimated as 3, 10 and 19 nm). DSC-Al curve is reproduced for comparison.

The threshold stress was found by plotting creep data as $\dot{\varepsilon}$ vs. $\sigma^{1/n}$, and extrapolating to $\dot{\varepsilon} = 0$ using a weighted least-squares linear regression [45]. Since diffusional creep is not active given the large grain size, we use here the experimentally-determined exponent for dislocation creep of pure aluminum, $n = 4.4$ [46], which is between the theoretical values for glide ($n = 3$ [47,48]) and climb ($n = 5$ [47,49]) and which has been used successfully in previous studies on DSC-Al without precipitates [7] and on Al–Sc(–Zr) alloys without dispersoids [17,18,20]. The threshold stresses for creep at 300 °C are listed in Table 1. Good linear fits were obtained for all samples, except for one case marked in Table 1. Also given in Table 1 are threshold values for DSC-Al and DSC-Al–Sc–Zr at 350 °C; data for DSC-Al–Sc are omitted due to coarsening of the precipitates (Fig. 1(b)).

Table 1
Aging treatment, estimated precipitate radius, apparent stress exponent and threshold stresses for creep experiments at 300 and 350 °C

Material	Aging treatment	Estimated radius (nm)	n_{ap} (–)	σ_{th} (MPa)
300 °C Creep Experiments				
DSC-Al	As-cast	0	18	59 ± 3
	450 °C/24 h	0	15	57 ± 2
DSC-Al–Sc	300 °C/24 h	3	13	97 ± 8
	As previous, crept 300 °C, aged 400 °C/24 h	10	21	86 ± 6
	As previous, crept 300 °C, aged 400 °C/24 h	19	20	84 ± 7
	300 °C/24 h	3	13	76 ± 3
	As previous, crept 300 °C, aged 450 °C/2 h	6	25	110 ± 20[a]
	As previous, crept 300 °C, aged 450 °C/24 h	30	22	91 ± 4
	300 °C/24 h	3	13	76 ± 3
	350 °C/24 h	4	13	79 ± 2
DSC-Al–Sc–Zr	300 °C/72 h	2	25	77 ± 2
	300 °C/72 h	2	26	77 ± 1
	350 °C/17 h	3	30	94 ± 7
	375 °C/3 h	8	25	78 ± 3
	350 °C/192 h	12	22	83 ± 2
	375 °C/48 h	24	21	85 ± 1
350 °C Creep Experiments				
DSC-Al	As cast	0	21	52 ± 1
	450 °C/24 h	0	20	52 ± 3
DSC-Al–Sc–Zr	350 °C/17 h	3	28	71 ± 3
	350 °C/17 h	3	25	75 ± 2
	375 °C/3 h	8	33	78 ± 2
	350 °C/192 h	12	26	79 ± 2

[a] Not plotted in Figs. 4 and 6 due to high error.

4. Discussion

4.1. Ambient temperature hardness

Fig. 1(a) and (b) shows that, in all four cases (aged at 300 and 350 °C, with and without Al_2O_3 dispersoids), the Zr-containing samples exhibit lower hardness than their Zr-free counterparts. This can be explained by the tendency, during aging, for most of the Zr atoms to remain in solid-solution while Sc precipitates, so that only a small amount of the Zr available in the alloy is found in the $Al_3(Sc_{1-x}Zr_x)$ precipitates. For example, it has been observed in Al–0.09Sc–0.047Zr that, after aging for 2412 h (~100 days) at 300 °C, the value of x is only 0.042 ± 0.007, indicating that Zr substitutes only 1 in 24 ± 4 Sc atoms in the precipitates [34]. Thus, the volume fraction of precipitates in the DSC-Al–Sc–Zr matrix is, to a good approximation, reduced to that of a Al–0.08 at.%Sc alloy and is lower than that of DSC-Al–Sc containing 0.11 at.%Sc. At 300 °C, the precipitate volume fractions in the matrix are thus 0.33 and 0.45 vol.%, respectively, as calculated from the lever rule. However, even at these low substitution levels, it is known that Zr is very effective at slowing the coarsening kinetics of the precipitates [43]. This is indeed observed in Fig. 1(a) and (b), which show no over-aging for DSC-Al–Sc–Zr, unlike DSC-Al–Sc which overages slightly at 300 °C and noticeably at 350 °C.

Although the nominal peak-aging times seem to differ among samples with and without Al_2O_3 dispersoids (e.g., 2 h for Al–Sc and 4 h for DSC-Al–Sc at 300 °C), the peak times are in fact undistinguishable when considering error bars on the hardness values in Fig. 1(a) and (b). This is confirmed by the conductivity curves for aging at 300 °C (Fig. 2(a) and (b)), which also show no significant difference between samples with and without Al_2O_3 dispersoids. The lack of influence of the incoherent Al_2O_3 particles upon the precipitation kinetics of Al_3Sc precipitates is in disagreement with several previous studies which found that ceramic particulates (with a wide range of size and volume fraction) accelerate precipitation [50–54]. This effect is often assigned to the presence of mismatch dislocations punched by the dispersoids into the matrix, which allow discontinuous nucleation and enhance growth of precipitates. However, other studies have shown that, for some matrix materials, aging is slowed or unaffected by dispersoids [53]. The lack of effect on the kinetics of precipitation observed in the present study may be due to the propensity for Al–Sc and Al–Sc–Zr alloys to exhibit a very high number density of homogenously nucleated precipitates [25,26,29,31,43,44], so that heterogeneous nucleation on mismatch dislocations produced by dispersoids does not contribute appreciably to the final number density. We thus assume in the following that the Al_2O_3 dispersoids do not alter the temporal evolution of Al_3Sc size, thus allowing for the direct comparison of specimens with and without Al_2O_3 at the same aging treatment.

Fig. 1(a) and (b) illustrates that the majority of the hardness of the DSC alloys originates from the Al_2O_3 dispersoids ($H_V = 1120 \pm 10$ MPa for DSC-Al). At peak-aging, however, the Al_3Sc precipitates boost hardness by ~50% (to $H_V = 1614 \pm 61$ MPa for DSC-Al–Sc aged at 300 °C), thus contributing a substantial fraction of the total hardness, despite a 100-fold smaller volume fraction (0.32 vol.% Al_3Sc in DSC-Al–Sc aged at 300 °C vs. 30 vol.% for Al_2O_3). This illustrates that the fine size of the precipitates (with mean radius of ~2 nm at peak aging [17–20,55], as compared to ~150 nm for Al_2O_3) is essential to their effectiveness as strengtheners in the alloy.

The overall strength τ_t of a material with various operative strengthening mechanisms, each with a characteristic strength increment τ_i, can be described by the empirical equation [19,56,57]:

$$\tau_t^k = \sum_i \tau_i^k \tag{3}$$

with an exponent $1 \leqslant k \leqslant 2$. All hardness values for DSC-Al–Sc fall within the upper and lower bounds for τ_t, given by exponents $k = 1$ (linear sum) and $k = 2$ (Pythagorean sum), respectively. A least-squares refinement gives $k = 1.30 \pm 0.05$ for DSC-Al–Sc and DSC-Al–Sc–Zr, and the resulting lines are given in Fig. 1(a) and (b). This value compares well with an earlier experimentally-determined value $k = 1.4$ for aluminum alloys with a bimodal distribution of precipitates [58].Other combinations of strengthening mechanisms provide different values for the exponent. For example, $k = 1$ was found for an aluminum alloy strengthened both by nanoscale Al_3Sc precipitates and Mg in solid-solution [19].

4.2. High temperature strength

4.2.1. Threshold stress

The threshold stresses at 300 and 350 °C listed in Table 1 for precipitate-free DSC-Al are in agreement with those in the literature [7]. DSC-Al–Sc(–Zr) alloys have significantly higher threshold stresses than DSC-Al or literature data for Al–Sc(–Zr) alloys [16–18,20]. This indicates that, as for hardness at ambient temperature, high-temperature strengthening occurs at both length scales, due to the two populations of nanometer-sized $Al_3(Sc_{1-x}Zr_x)$ precipitates and the submicrometer Al_2O_3 particles. This case is different from that considered by previous authors on dual-population strengthening [59–62], where the two populations consist of dispersoids impeding dislocations and supramicrometer reinforcements which strengthen the material by load transfer (rather than nanometer-size precipitates, as considered here, which also impeded dislocations).

The threshold stresses at 300 °C are plotted for all materials in Fig. 4 against the precipitate radius, estimated based on coarsening kinetics in Al–Sc [44] and Al–Sc–Zr [43] alloys. One micrograph by Marquis [63] for DSC-Al–Zr aged at 350 °C for 2 h confirms that these estimates are realistic. The threshold stress of DSC-Al–Sc(–Zr)

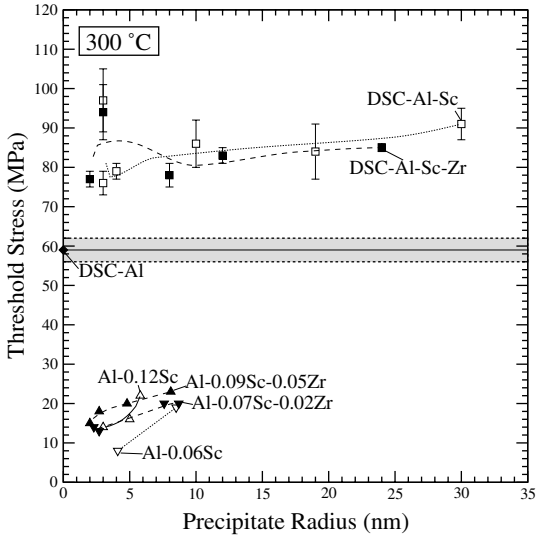

Fig. 4. Creep threshold stress at 300 °C as a function of estimated $Al_3(Sc_{1-x}Zr_x)$ radius for present DSC alloys as well as Al–Sc [17,18] and Al–Sc–Zr alloys [20] (compositions in at.%). Lines show trends.

shows a mildly increasing trend with aging time. A similar stronger trend exists for Al–Sc and Al–Sc–Zr alloys [20], as also shown in Fig. 4 and has been modeled previously by considering the elastic interactions between dislocations and precipitates [39]. Fig. 4 also shows that, within error, the threshold stresses for DSC-Al–Sc(–Zr) are equal to the sum of the threshold stresses for DSC-Al and Al–Sc-(–Zr). At first view, this is an unexpected result, as it may be expected that the overall threshold stress should be the higher of the threshold stress for the two active mechanisms. This prediction is based on the assumption that dislocation motion is impeded sequentially by each population of particles. Dislocations first climb over the many fine precipitates present between the larger dispersoids. Then, after they encounter and climb over a coarser dispersoid, they detach from it. As the two types of obstacles are overcome sequentially by the dislocations, the overall threshold stress is the higher of the two mechanisms, which is the detachment from the dispersoid in the present case. This approach predicts that the precipitates have no effect on the threshold stress of DSC-Al–Sc(–Zr), which is not supported by the experimental results (Table 1 and Fig. 4). The following section presents a possible explanation for this discrepancy.

4.2.2. Extension of the detachment model to include precipitate back-stress

Here, we consider that dislocation motion is impeded simultaneously, rather than sequentially, by both dispersoids and precipitates, which leads to a threshold stress higher than for a dislocation interacting with either type of particles, a trend in agreement with experimental data. This situation occurs when the dislocations are pinned at the departure side of the Al_2O_3 dispersoids (after having climbed over them), while concurrently being subjected to the elastic back-stress from nearby $Al_3(Sc_{1-x}Zr_x)$ precipitates. If that back-stress is negative, i.e., opposite in sign to the shear stress externally applied to the dislocations, it impedes the dislocation detachment process so that the overall threshold stress is the sum of the true detachment stress from the dispersoids and the back-stress from the nearby precipitates. If the former is expressed as a tensile value, σ_D, and the latter is expressed as a shear value, τ_B, the overall threshold stress in tension, σ_{th}, is

$$\sigma_{th} = \sigma_D + M\tau_B, \tag{4}$$

where M is the mean matrix orientation factor ($M = 3.06$ for Al [64]).

We do not seek to determine the tensile detachment threshold stress σ_D in DSC-Al, as this has been done previously by using the original detachment model [12,13] with the additional consideration of dislocation pileups [14]. Rather, we consider a dislocation pinned at the departure side of an Al_2O_3 dispersoid and calculate the shear back-stress τ_B acting on this detaching dislocation by the first four nearest neighbor $Al_3(Sc_{1-x}Zr_x)$ precipitates (totaling 10 nearest precipitates), with other farther precipitates assumed to have a negligible back-stress. The overall threshold stress can then be calculated from Eq. (4). As for a previous model [39], we consider stresses associated with lattice and modulus misfit of Al_3Sc precipitates in the Al matrix. We assume an idealized, highly simplified geometry, sketched in Fig. 5(a) and (b), where any segment of an edge dislocation pinned at the departure side of the dispersoid is subjected to the stress field of 10 neighboring precipitates. The precipitates are assumed to have a constant radius and to be arranged on a cubic lattice, as used previously [39]. Thus, no enrichment of precipitates around the dispersoid is assumed, as supported by the unchanged precipitation kinetics with and without Al_2O_3 dispersoids (Figs. 1 and 2).

As shown in Fig. 5(a), there are four main geometric parameters for the calculation of the back-stress: the precipitate radius R, the spacing λ between the precipitates, and the spacing δ and height h between the dislocation slip plane and the nearest precipitate. Assuming a cylindrical shape for the alumina dispersoid (with diameter and height D) allows us to use a constant distance δ between the dislocation pinned at the departure side of the dispersoid and the nearest row of precipitate, as shown in Fig. 5(b). Then, a segment of the dislocation pinned at the interface, with length λ, is representative of the whole pinned dislocation length (neglecting end segments near the edge of the dispersoid).

The first component of the back-stress is due to the lattice mismatch between the precipitates and the matrix. Any point on the segment of length λ of the straight edge dislocation (with Burgers vector normal to the x-axis) is subjected to a shear stress τ_ε [65]:

$$\tau_\varepsilon = \frac{6\mu_{Al}\varepsilon R^3}{r^5} yz, \tag{5}$$

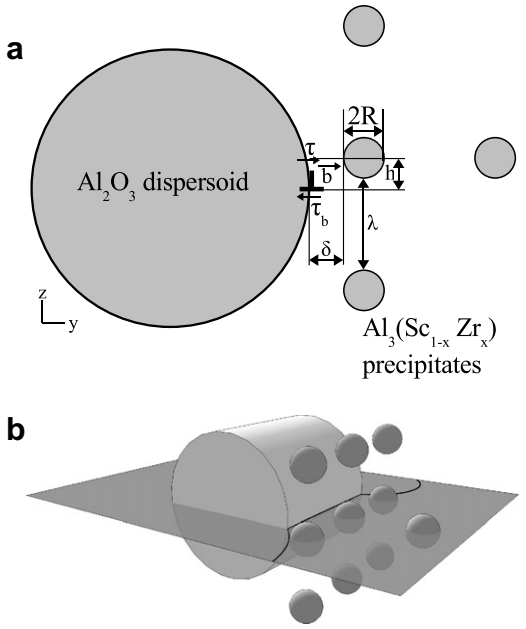

Fig. 5. Schematic of Al_2O_3 dispersoid and $Al_3(Sc_{1-x}Zr_x)$ precipitates illustrating the geometry used in the model. (a) Projection perpendicular to the dislocation glide plane. A dislocation detaching from the departure side of the dispersoid is subjected to an applied resolved shear stress, τ_B, and a back-stress, τ_B, imposed by an array of $Al_3(Sc_{1-x}Zr_x)$ precipitates. (b) Three-dimensional schematic, showing all 10 precipitates (3×3 planar array and additional precipitate) contributing to the back-stress on the dislocation.

where R is the precipitate radius and r is the distance from the center of the precipitate to the point on a dislocation (given by $r = (x^2 + y^2 + z^2)^{1/2}$, where x, y and z are the coordinates of the center of the precipitate if the point on a dislocation is at the origin) and μ_{Al} is the temperature-dependent matrix shear modulus (given as $\mu_{Al} = 25.4[1 - 0.5(T - 300)/933]$ with GPa units [46]). The temperature-dependent constrained lattice mismatch of the precipitate with the matrix, ε, is given by [65]

$$\varepsilon = \frac{\varepsilon'}{1 + \frac{4\mu_{Al}}{3\chi_{Al_3(Sc_{1-x}Zr_x)}}}. \tag{6}$$

In this equation, $\chi_{Al_3(Sc_{1-x}Zr_x)}$ is the bulk modulus of the precipitate (taken as 100 GPa [66–68]) and the unconstrained mismatch is given by $\varepsilon' = (a_{Al3(Sc,Zr)}/a_{Al}) - 1$ [69,70] with a_i as the temperature-dependent lattice parameter of phase i given by $a_i = a_{i0}(1 + \alpha_i(T - 300))$, where a_{i0} is the lattice parameter at 300 K for phase i ($a_{i0} = 0.4049$ nm for Al [46] and 0.4013 nm for Al_3Sc [32]) and α_i is the linear thermal expansion given in Ref. [70]. The Al_3Sc lattice parameter was used for both DSC-Al–Sc and DSC-Al–Sc–Zr (the latter because of the very small amount of Zr in $Al_3(Sc_{1-x}Zr_x)$ precipitates).

The second contribution to the back-stress on the detaching dislocation originates from the modulus mismatch between the precipitate ($\mu_{Al_3(Sc_{1-x}Zr_x)} = 68.0$ GPa [66]) and the matrix ($\mu_{Al} = 21.7$ GPa at 300 °C). For a dislocation in the matrix, it is given by τ_μ as

$$\tau_\mu = F_\mu b \lambda, \tag{7}$$

where $b = a_{Al}/\sqrt{2}$ is the magnitude of the Burgers vector, F_μ is the force acting on the dislocation and λ is the length of the dislocation segment under consideration. This length is taken as the inter-precipitate spacing, which can be calculated as [58]

$$\lambda = 2R\left(\sqrt{\frac{\pi}{4f}} - 1\right), \tag{8}$$

where f is the volume fraction of precipitates in the matrix calculated through the lever rule from the Al–Sc binary diagram for both Al–Sc and Al–Sc–Zr (the latter assuming 0.08 at.% Sc, thus ignoring the small amount of Zr in the precipitates). Because no simple exact solution exists for spherical or cylindrical particles, the two-dimensional (2D) solution given by Dundurs [71] for a circular precipitate interacting with a straight edge dislocation is used:

$$F_\mu = -R\frac{\partial E_\mu}{\partial y}, \tag{9}$$

where E_μ is a function of dislocation–precipitate distance, precipitate radius and elastic constants for Al and Al_3Sc, given in Refs. [39,71]. The above approach follows that used by Marquis and Dunand [39] to calculate the forces impeding the climb of dislocations around coherent precipitates. The modulus mismatch stresses are symmetric in the z-direction and always oppose detachment, but they are orders of magnitude lower than the lattice mismatch stresses for the present case (Al and Al_3Sc at 300 °C), so that the 2D modulus mismatch assumption is expected to introduce negligible errors in the final calculations.

The shear back-stress is the sum of the back-stresses from the lattice and modulus mismatches given by Eqs. (5) and (7):

$$\tau_B = -(\tau_\varepsilon + \tau_\mu), \tag{10}$$

where the negative sign is used because Eqs. (5), (7) and (9) define a repulsive stress (against the applied stress) with a negative sign, whereas in Eq. (4) a positive back-stress (which is repulsive) increases the threshold stress.

Eq. (10) was evaluated numerically and averaged over $-\lambda/2 < x < \lambda/2$ to obtain the average back-stress. Furthermore, z is set to $(R + \delta)\tan\theta$ and is averaged over the interval $0 < \theta < \pi/2$. The interval $-\pi/2 < \theta < 0$ is ignored since the anti-symmetric nature of τ_ε (which is much higher than τ_μ) provides a positive shear stress which helps the detachment of the dislocation. This is equivalent to considering that only half the dispersoids sampled by the dislocation during its glide through the matrix have a precipitate configuration which prevents detachment, with $h > 0$ and a repulsive τ_ε.

The only adjustable parameter is δ, the distance between the pinned dislocation and the nearest precipitate in the matrix (Fig. 5(a)). Computations were performed for a series of values ($\delta = b$, $\delta = 5b$ and $\delta = 10b$) and are plotted in Fig. 6. With increasing values of δ, the back-stress becomes

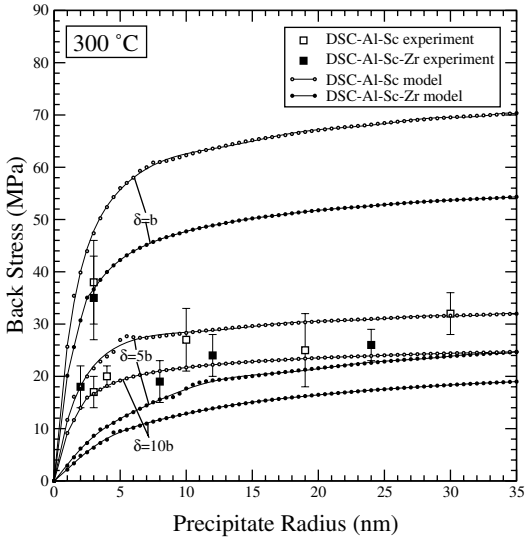

Fig. 6. Comparison between the calculated compressive back-stress (lines connecting individually calculated points) and the experimentally measured compressive threshold stress increments (large squares, found as difference between threshold stresses of DSC-Al–Sc(–Zr) and DSC-Al in Fig. 4) as a function of estimated precipitate radius.

smaller, as expected. We consider here the lowest range of δ values (within the possible range $b < \delta < \lambda/2$) because the dislocation sequentially bypasses a large number of obstacles placed in series and becomes pinned at those obstacles with lowest values of δ, where the back-stress is maximum. As shown in Fig. 6, the model seems to capture the main trend of the experimental data, i.e., the threshold stress increases with increasing precipitate radius R. The model also predicts a somewhat lowered threshold stress for DSC-Al–Sc–Zr as compared to DSC-Al–Sc, a trend that is too weak to be detectable within experimental errors.

Because of the many simplifications and assumptions made in the model, our aim is limited to seeking a conceptual understanding about the back-stress rather than achieving quantitative predictions. We thus do not seek here to improve the model by considering further refinements, e.g., enhanced density of precipitates around dispersoids or interactions between non-attached segments of the dislocation and precipitates. It is therefore perhaps fortuitous that a good quantitative agreement exists between the experimentally measured and numerically modeled threshold stresses for a value of $\delta = 5b$. Nonetheless, the model provides a simple explanation of the synergy observed in the creep threshold stress of DSC-Al–Sc, and by extension other metals, strengthened with two populations of coherent precipitates (providing a back-stress) and incoherent dispersoids (acting through a detachment stress).

5. Conclusions

This study examines dispersion-strengthened-cast aluminum (DSC-Al) containing two populations of particles: 30 vol.% submicron, incoherent Al_2O_3 dispersoids and 0.2–0.3 vol.% nanosize, coherent Al_3Sc precipitates (with and without small Zr additions in solid-solution). The following conclusions can be drawn.

- DSC-Al–Sc(–Zr) exhibits strengthening at ambient temperature from both the Al_3Sc precipitates and the Al_2O_3 dispersoids, as measured by microhardness and uniaxial compressive testing. The Al_3Sc precipitation kinetics are unaffected by the presence of Al_2O_3.
- Partial replacement of Sc with Zr in DSC-Al–Sc–Zr is the likely explanation for the observed lower peak hardness (due to lower volume fraction of precipitates) and elimination of over-aging at 300 or 350 °C (due to slower coarsening kinetics), as compared to DSC-Al–Sc.
- DSC-Al–Sc(–Zr) tested under compressive creep conditions at 300 and 350 °C exhibits high stress exponents, which are characteristic of materials with a threshold stresses (as also exhibited by DSC-Al and Al–Sc(–Zr) alloys).
- Partial replacement of Sc with Zr in Al–Sc–Zr and DSC-Al–Sc–Zr slightly decreases the creep-resistance and threshold stress, as expected from the decrease of volume fraction and lattice mismatch of the precipitates.
- The threshold stress of DSC-Al–Sc(–Zr) is greater than either that of precipitate-free DSC-Al or dispersoid-free Al–Sc(–Zr) alloys. This indicates that both populations of particles (precipitates and dispersoids) affect the threshold mechanism, despite their very different size, volume fraction and coherency with the matrix.
- This dual-strengthening effect is modeled by considering dislocations pinned at the departure side of Al_2O_3 dispersoids while being subjected to a back-stress from the nearby Al_3Sc precipitates, due to the strain field originating from their lattice and modulus mismatches with the matrix.

Acknowledgements

This research is supported by the US Department of Energy through grant DE-FG02-98ER45721. The authors thank Professor D.N. Seidman (Northwestern University (NU)) for useful conversations and Dr E.A. Marquis (NU, now at Sandia National Laboratories) for useful discussion and for casting the Al–Sc alloy. RAK was partially supported by a Walter P. Murphy Fellowship from NU.

References

[1] Cadek J. Creep in metallic materials. New York: Elsevier; 1998.
[2] Oliver WC, Nix WD. Acta Metall Mater 1982;30:1335–47.
[3] Clauer AH, Hansen N. Acta Metall Mater 1984;32:269–78.
[4] Rosler J, Joos R, Arzt E. Metall Trans A 1992;23:1521–39.
[5] Li Y, Langdon TG. Acta Mater 1997;45:4797–806.
[6] Pandey AB, Mishra RS, Paradkar AG, Mahajan YR. Acta Mater 1997;45:1297–306.
[7] Jansen AM, Dunand DC. Acta Mater 1997;45:4583–92.
[8] Mohamed FA. Mater Sci Eng A 1998;245:242–56.

[9] Ma ZY, Tjong SC. Compos Sci Technol 2001;61:771–86.
[10] Sherby OD, Taleff EM. Mater Sci Eng A 2002;322:89–99.
[11] Mukherjee AK, Bird JE, Dorn JE. ASM Trans Q 1969;62:155.
[12] Arzt E, Rosler J. Acta Metall Mater 1988;36:1053–60.
[13] Rosler J, Arzt E. Acta Metall Mater 1990;38:671–83.
[14] Dunand DC, Jansen AM. Acta Mater 1997;45:4569–81.
[15] Knipling KE, Dunand DC, Seidman DN. Z Metallkd 2006;97:246–65.
[16] Fuller CB, Seidman DN, Dunand DC. Scripta Mater 1999;40:691–6.
[17] Seidman DN, Marquis EA, Dunand DC. Acta Mater 2002;50: 4021–35.
[18] Marquis EA, Seidman DN, Dunand DC. Acta Mater 2003;51:285–7.
[19] Marquis EA, Seidman DN, Dunand DC. Acta Mater 2003;51: 4751–60.
[20] Fuller CB, Seidman DN, Dunand DC. Acta Mater 2003;51:4803–14.
[21] Deshmukh SP, Mishra RS, Kendig KL. Mater Sci Eng A 2004;381:381–5.
[22] Deshmukh SP, Mishra RS, Kendig KL. Mater Sci Eng A 2005;410–411:53–7.
[23] van Dalen ME, Dunand DC, Seidman DN. Acta Mater 2005;53: 4225–35.
[24] Karnesky RA, Seidman DN, Dunand DC. Mater Sci Forum 2006; 519–521:1035–40.
[25] Royset J, Ryum N. Int Mater Rev 2005;50:19–44.
[26] Toropova LS. Advanced aluminum alloys containing scandium: structure and properties. Amsterdam: Taylor & Francis; 1998.
[27] Blake N, Hopkins MA. J Mater Sci 1985;20:2861–7.
[28] Hyland RW. Metall Trans A 1992;23:1947–55.
[29] Novotny GM, Ardell AJ. Mater Sci Eng A 2001;318:144–54.
[30] Clouet E, Barbu A, Lae L, Martin G. Acta Mater 2005;53: 2313–25.
[31] Royset J, Ryum N. Mater Sci Eng A 2005;396:409–22.
[32] Harada Y, Dunand DC. Mater Sci Eng A 2002;329:686–95.
[33] Forbord B, Lefebvre W, Danoix F, Hallem H, Marthinsen K. Scripta Mater 2004;51:333–7.
[34] Fuller CB, Murray JL, Seidman DN. Acta Mater 2005;53:5401–13.
[35] Tolley A, Radmilovic V, Dahmen U. Scripta Mater 2005;52:621–5.
[36] Bergner D, van Chi N. Wissenschaftliche Zeitschrift der Padagogischen Hochschule 1977;15.
[37] Marumo T, Fujikawa SI, Hirano K. J Jpn Inst Light Met 1989;23:1.
[38] Fujikawa SI. Defect Diffus Forum 1997;143:115–20.
[39] Marquis EA, Dunand DC. Scripta Mater 2002;47:503–8.
[40] Rosler J, Arzt E. Acta Metall Mater 1988;36:1043–51.
[41] Redsten AM, Klier EM, Brown AM, Dunand DC. Mater Sci Eng A 1995;201:88–102.
[42] Han BQ, Dunand DC. Mater Sci Eng A 2000;277:297–304.
[43] Fuller CB, Seidman DN. Acta Mater 2005;53:5415–28.
[44] Marquis EA, Seidman DN. Acta Mater 2001;49:1909–19.
[45] Lagneborg R, Bergman B. Met Sci 1976;10:20–8.
[46] Frost HJ, Ashby MF. Deformation-mechanism maps: the plasticity and creep of metals and ceramics. Oxford: Pergamon Press; 1982.
[47] Mohamed FA, Langdon TG. Acta Metall Mater 1974;22:779–88.
[48] Weertman J. J Appl Phys 1957;28:1185–9.
[49] Weertman J. J Appl Phys 1957;28:362–4.
[50] Arakawa S, Hatayama T, Matsugi K, Yanagisawa O. Scripta Mater 2000;42:755–60.
[51] Gomez de Salazar JM, Barrena MI. Scripta Mater 2001;44: 2489–95.
[52] Unsworth JP, Bandyopadhyay S. J Mater Sci 1994;29:4645–50.
[53] Lloyd DJ. Int Mater Rev 1994;39:1–23.
[54] Goujon C, Goeuriot P. Mater Sci Eng A: Struct 2003;356:399–404.
[55] Karnesky RA, van Dalen ME, Dunand DC, Seidman DN. Scripta Mater 2006;55:437–40.
[56] Lagerpusch U, Mohles V, Baither D, Anczykowski B, Nembach E. Acta Mater 2000;48:3647–56.
[57] Lagerpusch U, Mohles V, Nembach E. Mater Sci Eng A 2001;319:176–8.
[58] Huang JC, Ardell AJ. Acta Metall Mater 1988;36:2995–3006.
[59] Cadek J, Kucharova K, Milicka K. J Alloys Compd 2004;378:123–6.
[60] Peng LM, Zhu SJ. Int J Mater Prod Technol 2003;18:215–54.
[61] Rosler J, Baker M. Acta Mater 2000;48:3553–67.
[62] Kucharova K, Cadek J, Zhu SJ. J Mater Sci 2003;38:3535–43.
[63] Marquis EA. Ph.D. Thesis, Northwestern University, 2002.
[64] Meyers MA, Chawla KK. Mechanical metallurgy: principles and applications. Englewood Cliffs, NJ: Prentice-Hall; 1984.
[65] Nembach E. Particle strengthening of metals and alloys. New York: Wiley; 1997.
[66] Hyland RW, Stiffler RC. Scripta Metall Mater 1991;25:473–7.
[67] Hyland RW, Asta R, Foiles SM, Rohrer CL. Acta Mater 1998;46: 3667–78.
[68] Zhang XD, Sauthoff G. Intermetallics 1995;3:137–40.
[69] Harada Y, Dunand DC. Scripta Mater 2003;48:219–22.
[70] Royset J, Ryum N. Scripta Mater 2005;52:1275–9.
[71] Dundurs J. Elastic interaction of dislocations with inhomogeneities. In: Mura T, editor. Mathematical theory of dislocations. New York: ASME; 1969. p. 70–115.